EFFECT OF SiC PARTICLE SIZE ON THE MATERIAL AND MECHANICAL PROPERTIES OF MULLITE BONDED SiC CERAMICS PROCESSED BY INFILTRATION TECHNIQUE

SANCHITA BAITALIK, #NIJHUMA KAYAL, ATANU DEY, OMPRAKASH CHAKRABARTI

Central Glass and Ceramic Research Institute, CSIR, 196, Raja S. C. Mullick Road, Kolkata-700 032, India

#E-mail: nijhuma@cgcri.res.in

Submitted October 14, 2014; accepted December 23, 2014

Keywords: Particle size, Mullite bond, Infiltration, Porous SiC, Microstructure

The influence of SiC particles size on the bonding phase content, microstructure, SiC oxidation degree, flexural strength, porosity and pore size distribution of mullitebonded porous SiC ceramics were studied and compared with oxidebonded porous SiC ceramics. The SEM morphologies and EDS elemental analysis results showed the presence of needle shaped crystals of mullite and fish scaled cristobalite in the bond phase. It was found that increase of SiC particle size effectively enhanced the porosity and decreased the strength. The porosity decreased as the size of SiC particles decreased from 36 vol. % at 99 μm to 25 vol. % at 4.47 μm. The oxidation degree of SiC was found to be reduced by infiltration of mullite precursor sol and enhanced with sintering temperature. Bimodal pore size distributions were obtained for mullite-bonded porous SiC ceramics and the average pore diameter varied in the range of 2 - 30 μm with variation of particle size.

INTRODUCTION

Currently, porous SiC ceramics have been a focus of interesting research in the field of porous materials due to their unique combination of properties such as high strength, high hardness, and superb mechanical and chemical stabilities, particularly at high temperatures and hostile atmospheres, high thermal conductivity, low thermal expansion coefficient, etc. Hence porous SiC ceramics have been considered as an ideal candidate for catalyst supports, thermal insulators, high temperature structural materials, kiln furniture, and hot gas particulate systems in different industrial processes like integrated gasification combined cycle (IGCC) and coal combustion [1-4]. The processing methods used for the preparation of porous ceramics are mainly replica, sacrificial template, direct foaming and reaction bonding [5, 6]. All these methods require a very high temperature due to the strongly covalent nature of the Si–C bond, selective sintering additives, expensive atmosphere, costly equipment and delicate instrumentation [7]. Moreover during operation at high temperature this type of porous material (filter) fails as a result of oxidation of SiC especially in presence of water vapor [8]. To overcome these disadvantages, She et al. introduced *in-situ* reaction bonding [9], in which porous powder compact of SiC and alumina was heat treated in air to promote oxidation and consequently to bind SiC particles by oxidation derived SiO_2 glass and mullite formed by reaction of alumina and silica. Following this work several other workers reported series of oxide bonded (mullite, cordierite, etc) porous SiC ceramics [10-12]. Though the oxidation bonding methods were successful in forming oxide bonded porous SiC ceramics at low temperature, they were found to have several disadvantages as oxidation of SiC is limited in the depth of the zone hence limited for large scale production and mechanical failure of the final ceramics occurs due to inhomogeneous mixing of fine sintering aids. To avoid those problems our group prepared mullite bonded porous SiC ceramics following incorporation of sol-gel bond phase precursor by infiltration techniques to ensure a homogeneous distribution of the bond phase [13-14]. For the application of porous ceramics as a gas filter, a desired pore size and porosity with sufficient mechanical strength is needed to achieve high filtration efficiency. This could be achieved by controlling the size and amount of pore forming agent, powder compaction pressure, sintering temperature and time, etc. [15]. On the other hand, the pore diameter of porous ceramics can also be varied by varying the size of the starting powders. The purpose of this paper is to investigate, how the SiC particle size and sintering temperature influence the porosity, pore sizes and flexural strength of mullite bonded porous SiC (MBSC) ceramics where the mullite precursor sol is incorporated by an infiltration route. The properties were also compared with non-infiltrated samples that is only oxidation derived silica bonded SiC (SBSC) ceramics.

EXPERIMENTAL

Commercial SiC powder (Grindwell Norton, India) of three different particle sizes defined as fine (d_{50} = = 4.47 μm), medium (d_{50} = 51.77 μm) and coarse (d_{50} = = 99 μm) were used in this study, the characteristics of powders are listed in Table 1. XRD patterns of SiC powders are shown in Figure 1, indicating crystalline α-SiC phase (hexagonal crystal system ; space group: P63mc; unit cell parameters: $a = b = 3.0810$ Å, c = = 15.1200 Å and $a = b = 90°$ and $g = 120°$). The SiC particles were of irregular shape with non-uniform distribution of size as shown in Figure 2. The powders were mixed with 15 wt. % solution of polyvinyl alcohol binder

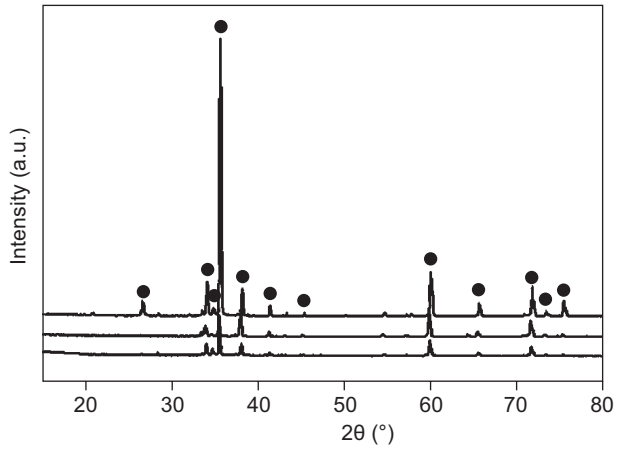

Figure 1. XRD pattern of different SiC particles: fine (top), medium (middle) and coarse (bottom) (● = SiC).

(Loba Chemie, India) and pressed in a hydraulic press to produce rectangular green bars (50 × 20 × 16 mm^3). The bars were dried and subsequently fired in air at 1100°C for 4 h for making the bars strong through the development of necks between the contacting particles. The bars were evacuated and further infiltrated with a liquid precursor of mullite following the procedure described in our previous paper [14]. The infiltrated samples were dried at 100°C to remove the solvent, and the process was repeated. The infiltrated and non-infiltrated samples were finally sintered in air at 1300 - 1500°C for 4 h in an electrically heated ceramic tube furnace (Model No.-TE-3499-2, M/S Therelek Engineers (P) Ltd., Bangalore, India) to obtain mullite and silica bonded porous ceramics respectively. The final ceramics were characterized by measurement of density and porosity by the water immersion method, identification of crystalline phases by XRD analysis (PW1710, Philips, The Netherlands) using Cu-Ka radiation of wavelength l = 1.5406 Å and determination of the pore size distribution (PSD) by Hg-intrusion porosimetry (Pore-master, Quantachrome Instruments Inc., Florida, USA). The quantitative analysis was done by the Rietveld technique using the High Score Plus software (version 3.0e, PANalytical B.V., The Netherlands). The room temperature flexural strength was determined in three-point mode (with a span of 40 mm, speed of 0.5 mm·min^{-1}, sample crosssection of 4.75 by 3.25 mm^2; samples were ground and polished up to 10 mm finish and tensile surfaces were champhered) using an Instron Universal Testing machine. The deflection was monitored through a LVDT with a resolution of 0.05 % of full scale

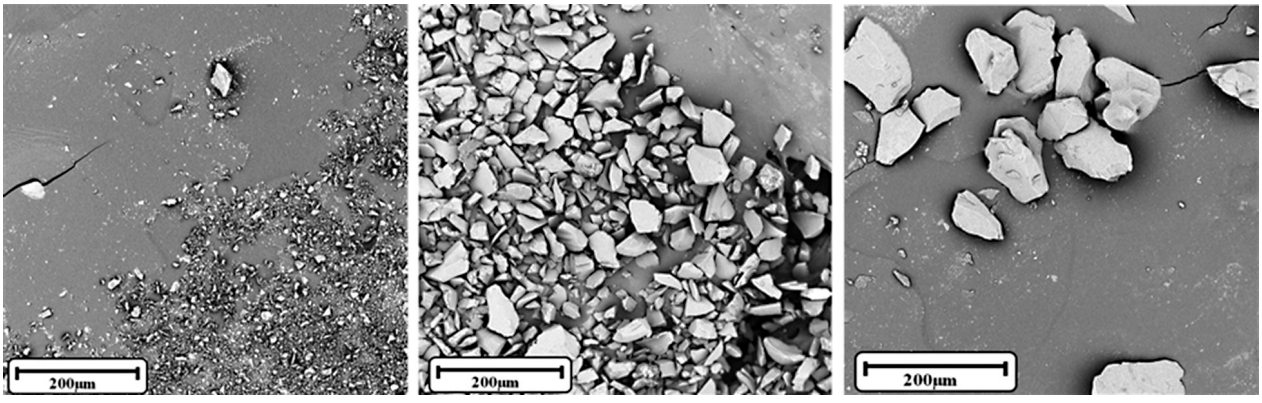

a) b) c)

Figure 2. Micrographs of fine (a), medium (b) and coarse (c) SiC powders.

Table 1. Characteristics of SiC powders.

Type of SiC powder	Particle size distribution (μm)			Chemical composition (w/w %)			
	d_{10}	d_{50}	d_{90}	SiC	$Si+SiO_2$	Free C	Fe_2O_3
Fine	1.12	4.47	10.95	91.00	6.00	1.00	0.30
Medium	26.91	51.77	93.43	95.00	3.50	0.50	–
Coarse	57.33	99.00	155.80	96.00	2.50	0.50	–

deflection and from the load-deflection data the Young's modulus was determined with the help of a standard software (Instron Bluehill-2, UK). The averages of five readings were reported as final mechanical property data. Microstructure was examined by the scanning electron microscopic (SEM) technique (SE-440, Leo-Cambridge, Cambridge, UK).

RESULTS AND DISCUSSION

Mullite sol infiltration into powder compact

Samples heat-treated at 1100°C were found to be strong with no sign of corner breakage and surface cracks. The samples exhibited weight gain in the range of 0.1 - 7.0 wt. % due to oxidation of SiC particles which decreased with increasing particle size due to the decrease of surface area. A small piece of bar was cut from a sample heat-treated at 1100°C and suspended in mullite sol by a wire attached to an electric balance to measure the infiltrated weight gain as a function of time. The fractional infiltrated weight gain was plotted against sqare root of time ($t^{1/2}$) as presented in Figure 3. Initially the rate of infiltration sharply increased and after a certain time the rate became slow. According to the available literature reports [16, 17] on the infiltration behaviour of liquid through porous media, initial infiltration is governed by the capilary force following Darcy's law and in later stage compressed air diffuses through the porous media following Fick's law. The capilary infiltration rate was found to be 5×10^{-2} $s^{1/2}$ and 6.69×10^{-2} $s^{1/2}$, respectively, for samples prepared with medium and coarse SiC powders. The infiltration rate at the second stage was observed to be 5.59×10^{-4} $s^{1/2}$ and 7.99×10^{-4} $s^{1/2}$, respectively, for samples prepared with medium and coarse SiC powders. Previously we studied the infiltration kinetics of mullite precursor sols into powder compacts prepared with SiC powders of d_{50} = = 22.4 μm and obtained infiltration rates 4.1×10^{-2} $s^{1/2}$ and 8.3×10^{-4} $s^{1/2}$, respectively, for the first and second stage of infiltration [14]. Although initial results indicated that the fractional volume infiltrated increased with decrease of SiC particle size, the final effect of particle size on infiltration rate was insignificant.

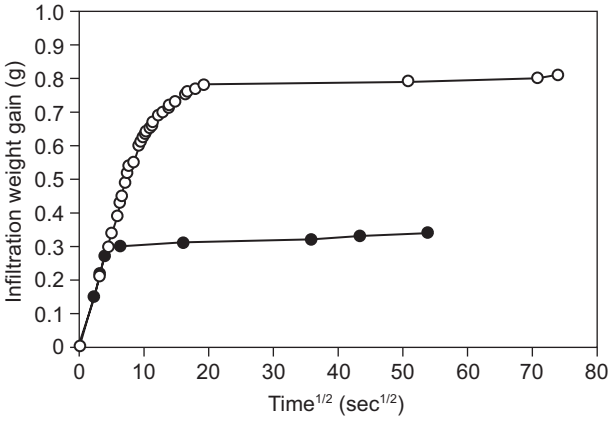

Figure 3. Plot of infiltrated weight gain by mullite precursor sol into 1100°C SiC bar samples prepared with medium (○) and coarse (●) SiC powder against (time)$^{1/2}$ at 0.58 and 0.56 relative density respectively.

Mullite sol was incorporated by repeated infiltration into bar-shaped specimens fired at 1100°C followed by drying. Infiltration weight gain data are presented in Figure 4. After the seventh infiltration there was no significant increase of weight gain. In the seventh cycle the infiltration mass gain was found to vary between 22 and 22.30 wt. %, irrespective of the starting SiC particle sizes. The mass gain after the sixth infiltration became insignificant, probably because of clogging of the pore channels.

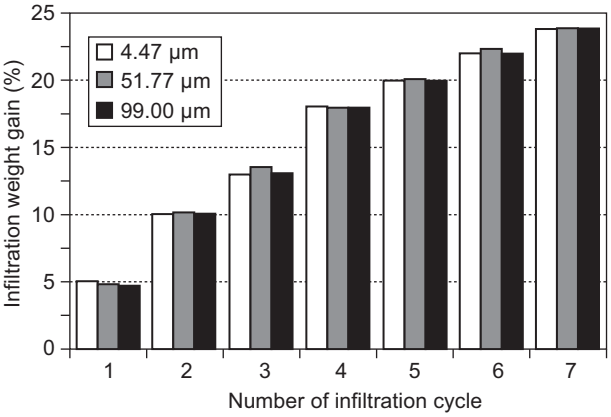

Figure 4. Effect of infiltration cycle on weight gain (%) SiC samples prepared from different particle sizes at 1.74 g/c.c, 1.84 g/c.c and 1.81 g/c.c bar density respectively.

Material property and microstructure

Both the infiltrated and non-infiltrated sintered ceramics exhibited no distortion in shape. No sign of crack and disintegration was noticed on the surfaces of the sintered samples except for the samples prepared from fine SiC powders sintered at 1500°C. The porosity for both MBSC and SBSC ceramics was found to decrease with an increase of sintering temperature and a decrease in particle size of SiC. Porosities of the oxide bonded ceramics of non-infiltrated samples were slightly lower compared to the MBSC ceramics which was due to higher bulk density of oxidation derived silica. The porosity of MBSC ceramics prepared at 1500°C increased from 25 to 36 vol. % with increase of SiC particle size from fine to coarse.

During sintering of the infiltrated samples, SiC oxidizes and forms silica. The degree of oxidation (*f*) of SiC was calculated by the method as described in our previous paper [14]. The degree of SiC oxidation of the sintered ceramics is presented in Figure 5. The percentage oxidation degree of SiC increased with

increase of sintering temperature and decrease of SiC particle size. Due to infiltration the % SiC oxidation degree is reduced from 53.60 to 40.60, 14.25 to 9.01 and 5.35 to 3.40 for SiC ceramic prepared at 1300°C using fine, medium and coarse SiC powders, respectively. A similar trend was also observed for samples prepared at 1500°C, where the % SiC oxidation degree decreased from 29.05 to 17.40 for samples prepared with medium SiC powder. Oxidation is faster for smaller size particles which may be due the to higher specific surface area and lower packing density. Similar results were also reported by Quanli et al., who observed that the weight and rate constant increased and oxidation activation energy decreased with decreasing particle size of SiC powders [18]. She et al. also observed an increase of silica content with decreasing particle size of SiC [19]. The reduction in the % SiC oxidation degree by infiltration was due to partial covering of effective surface area by mullite sol. We have theoretically calculated the vol. % of mullite in sintered ceramics following the procedure described in our previous paper [20]. The mullite concentration varied between 5 - 8 vol. % in the sintered ceramic samples. The higher vol. % of silica in SBSC compared to MBSC ceramics caused the decrease of porosity in SBSC ceramics. The porosity varied in the range 26 - 36 vol. % and 21 - 35 vol. % for MBSC and SBSC ceramics, respectively. Furthermore, during heating of the green compacts, organic groups in the dried mullite gel burned out, which also influenced the porosity increase in MBSC ceramics.

XRD scans of mullite bonded SiC ceramics sintered at 1500°C are presented in Figure 6. SiC, mullite and cristobalite were detected as the major crystalline phases. The crystalline phases detected in SBSC samples were SiC (crystal system: hexagonal; space group: P63mc; $a = b = 3.0817$ Å, $c = 15.1183$ Å and $a = b = 90°$ and $g = 120°$; JCPDS 49-1428) and cristobalite (crystal system: tetragonal; space group: P41212; $a = b = 4.9640$ Å, $c = 6.9200$ Å and $a = b = g = 90°$; JCPDS 76-0936) are shown in Figure 7. The crystal structures of SiC and cristobalite were the same in MBSC ceramics; in addition, mullite phase was detected with the chemical formula of $Al_6O_{13}Si_2$ and orthorhombic crystal system (space group: Pbam; $a = 7.5456$ Å, $b = 7.6898$ Å and $c = 2.8842$ Å and $a = b = g = 90°$; JCPDS 15-0776).

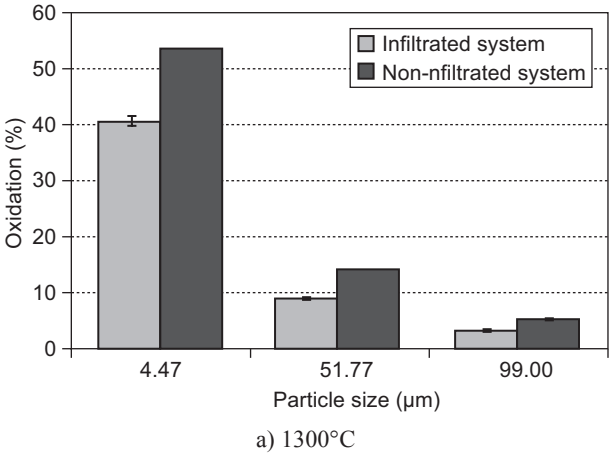

a) 1300°C

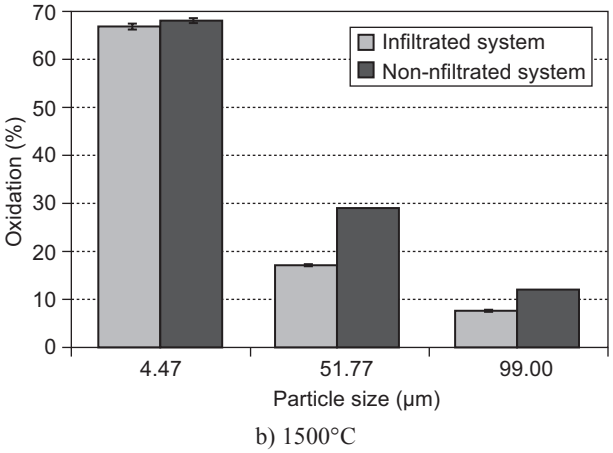

b) 1500°C

Figure 5. Plot of % SiC oxidation degree with variation of particle size for MBSC and SBSC ceramics prepared at (a) 1300°C and (b) 1500 °C.

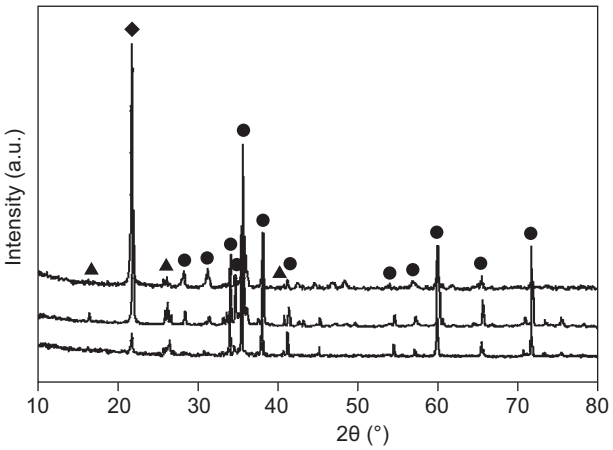

Figure 6. XRD scan of mullite bonded SiC sintered at 1500°C showing crystalline phases; mullite (▲), SiC (●) and Cystobalite (♦); fine (top), midium (middle) and coarse (bottom).

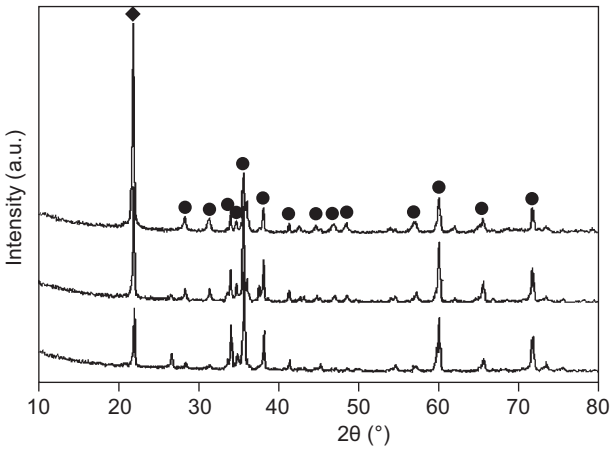

Figure 7. XRD scan of silica bonded SiC sintered at 1500°C showing only SiC (♦) and crystobalite (●) crystalline phases; fine (top), midium (middle) and coarse (bottom).

Figure 8 shows representative microstructures of MBSC ceramics. Interconnected porous networks are evident in the microstructures. The SiC particles are also seen to be bonded to each other at the contacting regions. The micrograph of MBSC ceramics at high magnification shows the needle shaped mullite crystals and cristobalite with fish-scale morphology. Energy dispersive X-ray (EDX) analysis during microstructure examination under back scattered electron (BSE) mode revealed some details about the presence of different elements in these areas and the results are shown in Figure 9. Cristobalite with fish-scale morphology is also observed in the microstructure of silica bricks. The cristobalite has the characteristic fish-scale morphology arising from the grain boundaries of the original quartz grains [21]. Needle-like crystals of mullite were observed by many researchers. Viswabaskaran et al. observed the presence of needle-shaped mullite crystals in the heat-treated compacts of kaolinite clay, reactive alumina and MgO [22]. Miao observed the formation of mullite crystals of needle-like morphology in the calcined powder compacts of natural topaz [23]. The results of EDX analysis confirmed the presence of Al, Si and O (the elemental constituents of mullite) in the areas of needle-shaped grains (region "a"). Examination of morphology and analysis of EDX results thus suggest that the needle-shaped grains were of mullite. The EDX result also showed the presence of Si and O (elements present in cristobalite) in the region "b". Morphological observations and EDX results thus suggest that the region "b" was cristobalite. However, in the EDX analysis of region "b" small amounts of Al and Fe were also detected; it was likely that the signal was coming from the region near or below the fish-scale morphology. In the present study the mullite crystals were seen to be of 2 - 6 μm in length and 0.5 - 1.0 μm in width. Lee et al. prepared mullite crystals from precursor at 1600°C and observed 1 - 2 μm in width and 10 - 20 μm in length [24]. The individual cristobalite grain size was found to be 2.30 μm in diameter. Damby et al. also reported fish-scale morphology of cristobalite of diameter 8 μm in volcanic ash produced from dome forming eruption [25].

The mullite bonded porous SiC ceramics exhibited bimodal pore size distribution for all particle sizes of SiC with different levels of porosity due to wide variation of distribution in the SiC particle size. The pore size distributions of MBSC ceramics sintered at 1500°C are shown in Figure 10. As the pores are mainly created by stacking of SiC particles, porosity and pore size increased with increasing starting SiC particle sizes. The average pore diameter of the main peak for MBSC ceramics

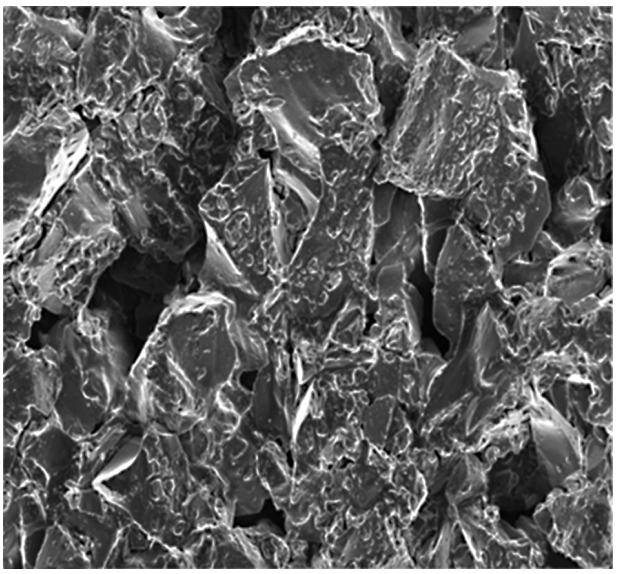

a)

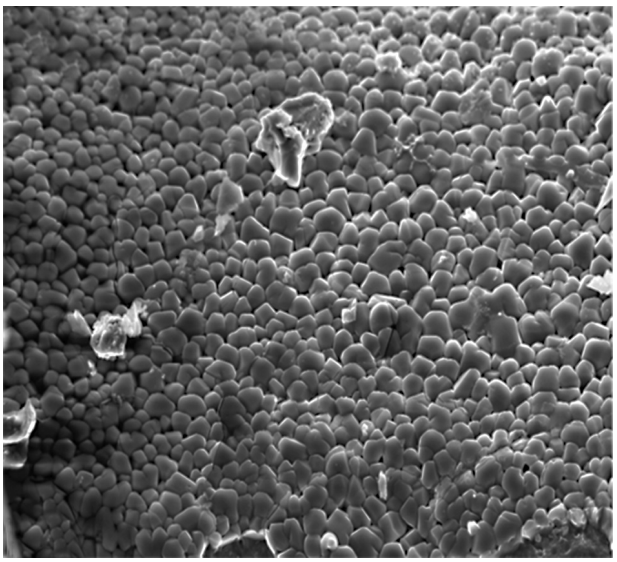

b)

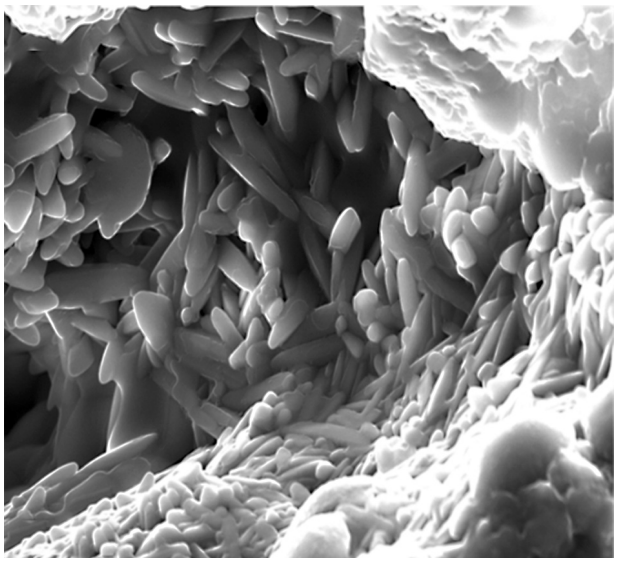

c)

Figure 8. SEM micrographs of MBSC ceramics made from coarse SiC powders clearly showing the (a) porus network; higher magnification showing (b) fish scale morphology of cristobalite (c) needle shape crystals of mullite.

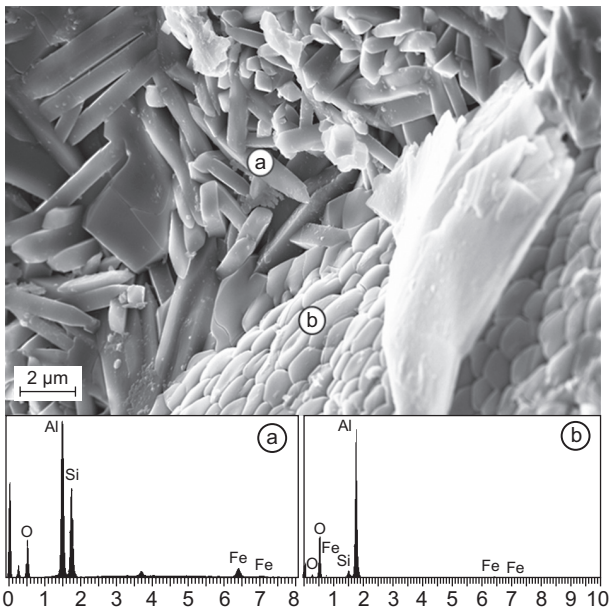

Figure 9. EDX results showing elemental information of different phases obtained during SEM microscopy of MBSC ceramics made from coarse SiC powders.

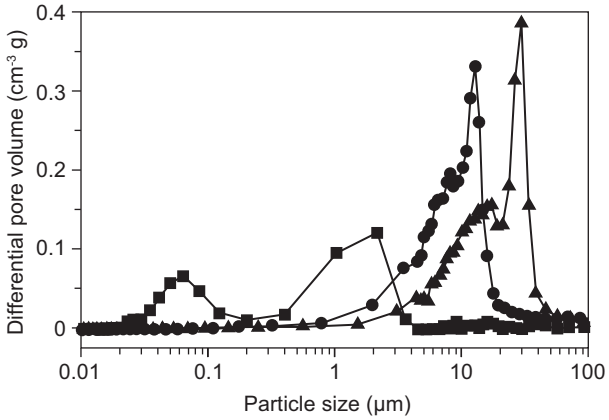

Figure 10. Pore size distribution graph of MBSC composites were fired at 1500°C showing bimodal pattern for SiC particle sizes; fine (■), medium (●) and coarse (▲).

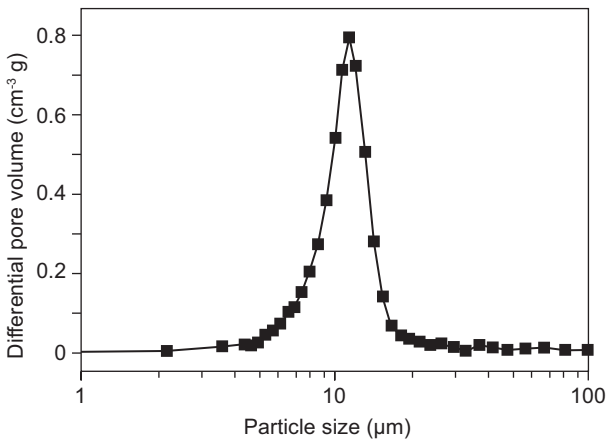

Figure 11. PSD pattern of SBSC ceramics prepared from medium size SiC powder sintered at 1300°C.

sintered at 1500°C were found to be 2.13, 12.58 and 29.89 μm, respectively, for the samples prepared using fine, medium and coarse SiC powder. Similar bimodal size distributions were also obtained for the MBSC ceramics sintered at 1300°C , and no significant change in the average pore diameter value was observed. For SBSC ceramics a monomodal pore size distribution was obtained for samples prepared from medium and coarse SiC powders. A typical pore size distribution of SBSC ceramics prepared from medium size SiC powder sintered at 1300°C is presented in Figure 11, in which the average pore diameter was found to be 11.50 μm. Small pores generated in case of MBSC ceramics might be filled up by the excess silica in case of SBSC ceramics. In our earlier work an average pore diameter of ~8 mm was achieved for the MBSC ceramics prepared using SiC powder of d_{50} = 22.4 μm [14]. She et.al reported the average pore diameter of 7 and 12 μm respectively for the OBSC ceramics prepared using SiC particle sizes 27 and 58 μm [26]. Lee et al. reported average pore diameter of 44 - 65 μm for oxide bonded porous SiC ceramics prepared using SiC particle sizes 180 μm [27] .

Mechanical Property

Figure 12 shows the effect of SiC particle size on the flexural strength of MBSC ceramics. The flexural strength was found to decrease with increasing SiC particle size. As the oxidation is enhanced with decreasing SiC particle size, there is an increased formation of cristobalite, which strengthens the bonding of SiC particles, and as a consequence the strength is improved. A maximum flexural strength of 39 MPa was obtained for MBSC ceramics with porosity 33.50 vol. % prepared from medium size SiC powders sintered at 1500°C. However the MBSC ceramics prepared from fine SiC powders sintered at 1500°C contained excessive contents of glassy phase, lead to crack formation, and thus strength was not measured. The flexural strength

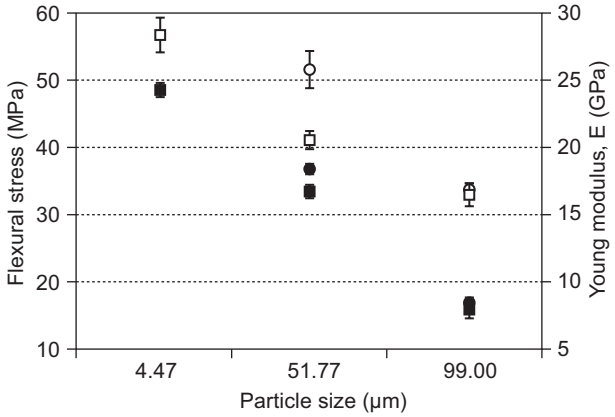

Figure 12. Particle size dependence of Flexural strength (● – MBSC; ■ – SBSC) and Young's Modulus (○ – MBSC; □ – SBSC) of porous SiC ceramics sintered at 1300°C and 1500°C.

of MBSC ceramics prepared from medium and coarse SiC powder was higher compared to the SBSC ceramics inspite of higher porosity in case of MBSC ceramics. An improved level of mixing of mullite sol and bonding of SiC particles firmly by needle-shaped mullite crystals as well as a decrease in mass gain due to silica obviously improved the mechanical properties of the MBSC ceramics. Values reported in the literature for the flexural strength of MBSC with no additives were 9.8 MPa at 50 % porosity, [28] 24 MPa at 43 % porosity, 39 MPa at 36 % porosity and 45.49 MPa at 29.54 % porosity [29]. The conditions used in the literature were particle sizes of 0.5 - 20 μm, sintering temperature of 1450 - 1550°C and compaction pressure of 30 - 90 MPa. Recently Ebrahimpour et al. reported [12] flexural strength of 40.6 MPa at 35 % of porosity for MBSC ceramics prepared at 1500°C from 11.1 μm SiC powder, 20 wt. % alumina sol and 15 wt. % alumina powder. The higher strength in the present MBSC ceramics can be attributed to the combined effect of incorporation of bond phase by infiltration and the bonding of SiC particles both by cristobalite and mullite.

CONCLUSIONS

In this study the effect of SiC particle size on the porosity, pore sizes and flexural strength of mullite bonded porous SiC ceramics were studied and compared with non-infiltrated samples, i.e. oxidation derived silica bonded SiC. Mullite bonded porous SiC ceramics were synthesized by an infiltration-based processing consisting of intrusion of monophasic mullite precursor sol into a porous compact of SiC followed by sintering at 1300 - 1500°C in air. The % SiC oxidation degree decrea-sed with decrease of sintering temperature, increase of SiC particle size and also by infiltration. Due to infiltration the % SiC oxidation degree is reduced from 53.60 to 40.60 for SiC ceramics prepared from SiC particles of d_{50} = 4.47 μm sintered at 1300°C. The mullite bonded porous SiC ceramics exhibited bimodal pore size distributions, whereas silica bonded porous SiC ceramics exhibited a monomodal pore size distributions. The average pore diamter was found to increase with increasing SiC particle size. Apart from SiC, mullite and cristobalite were detected as the major crystalline phases in the MBSC ceramics, while in SBSC ceramics mullite was not detected of course. The sintered ceramics were seen to have an interconnected open porous network. Needle shaped mullite crystals and cristobalite with fish-scale morphology were seen to be present with well developed necks that bond the SiC particles together. The porosity and flexural strength was found to be dependent on the SiC particle size, infiltration of mullite precusor sol and sintering temperature. A maximum flexural strength of 39 MPa was obtained for MBSC ceramics with porosity 33.50 vol. % prepared from SiC powders of d_{50} = 51.77 μm sintered at 1500°C.

Acknowledgment

The authors would like to thank Department of Science and Technology (DST), India for financial support (GAP 0239). Co-operation of Mr. S.K. Dalui of NOCCD, CGCRI, for performing the mechanical characterization is acknowledged with thanks.

REFERENCES

1. Judkins R. R., Stinton D. P., DeVan J. H.: J. Eng. Gas Turbines Power *118*, 500 (1996).
2. Keller N., Pham-Huu C., Roy S., Ledoux M. J., Estournes C. and Guille J.: J. Mater. Sci. *34*, 3189 (1999).
3. George Wei C., Oak Ridge T. N.: US Pat. No. 4481179, 6 November 1984.
4. Alvin M. A.: Ind. Eng. Chem. Res. *35*, 3384 (1996).
5. Studart A. R., Gozenbach U. T., Tervoort E., Gauckler L.: J. Am. Ceram. Soc. *89*, 1771 (2006)
6. Kumar B. V. M., Kim Y-W.: Sci. Technol. Adv. Mater. *11*, 044303 (2010).
7. Sigl L. S., Kleebe H. J.: J. Am. Ceram. Soc. *76*, 773 (1993).
8. Pastila P. H., Helanti V., Nikkila A. P., Mantyla T. A.: J. Eur. Ceram. Soc. *21*, 1261 (2001).
9. She J. H., Deng Z. Y., Doni J. D., Ohji T.: J. Mater. Sci. *37*, 3615 (2002).
10. Ding S., Zhu S., Zeng Y. P., Jiang D.: J. Eur. Ceram. Soc. *27*, 2095 (2007).
11. Liu S., Zeng Y. P., Jiang D.: Ceram. Int. *35*, 597 (2009).
12. Ebrahimpour O., Dubois C., Chaouki J.: J. Euro. Ceram. Soc. *34*, 237 (2014).
13. Dey A., Kayal N., Chakrabarti O.: Ceram. Int. *37*, 223 (2011).
14. Kayal N., Dey A., Chakrabarti O.: Mater. Sci. Eng. A *535*, 222 (2012).
15. Li J., H. Lin, J. Li: J. Euro. Ceram. Soc. *31*, 825 (2001).
16. Tu W. C., Lange F. F.: J. Am. Ceram. Soc. *78*, 3277 (1955).
17. Dullien F. A.: *Porous media-fluid transport and pore structure*, Academic Press, New York (1979).
18. Quanli J., Haijun Z., Suping L., Xiaolin J.: Ceram. Int. *33*, 309 (2007).
19. She J. H., Yang J. F., Kando N., Ohji T.: J. Am. Ceram. Soc. *85*, 2852 (2002).
20. Kayal N., Dey A., Chakrabarti O.: Mater. Sci. Eng. A *556*, 789 (2012).
21. Almarahle G.: Am. J. Appl. Sci. *2*, 465 (2005).
22. Viswabaskaran V., Gnanam F. D., and Balasubramanian B.: Appld. Clay Sci. *25*, 29 (2004).
23. Miao X.: Mater. Lett. *38*, 167 (1999).
24. Lee J., Kim J., Jung Y., Jo C., Paik U.: Ceram. Int. *28*, 935 (2002).
25. Damby D. E., Llewellin E.W., Horwell C. J., Williamson B. J., Najorka J., Cressey G., Carpenter M.: J. App. Cryst. *47*, 1205 (2014).
26. She J. H., Ohji T., Kanzaki S.: J. Euro. Ceram. Soc. *24*, 331 (2004).
27. Woo S.K., Lee K.S, Han I.S., Seo D.W, Park Y.O.: J. Ceram. Soc. Jpn. *109*, 742 (2001).
28. Ding S., Zhu S., Zeng Y., Jiang D.: Ceram. Int. *32*, 461 (2006).
29. Ding S., Zeng Y. P., Jiang D.: Mater. Sci. Eng. A. *425*, 326 (2006).